

Computational Fluid-Structure Interaction Of Axial Pipe Waves And Application Towards Bruce 'A' NGS Flow-Induced Feeder Vibration – Phase 1

E. D. Davidge¹, J. Goldberg², and M. Upton²

¹ Kinectrics Inc., Toronto, Ontario

² Bruce Power NSAS, Toronto, Ontario

Abstract

Work was completed which compared predicted fluid-structure interaction results with published experimental results. The model used an impact force to induce stress and pressure waves along a straight pipe which was sealed and filled with pressurized water. Local strain and pressure values at several locations are plotted against time and are presented for visual comparison. The predicted results compare well with the published results and many of the major interaction effects are clearly observable. Application in subsequent work towards Bruce 'A' flow-induced feeder vibration is discussed.

1. Introduction

Bruce Power has predicted feeder vibration issues will arise in the defuelling of selected channels in their reactors. When a channel is defueled, the flow rate through it increases due to the removed fuel, and feeder vibrations increase due to flow-induced vibration (FIV) and pump pressure pulses.

The current methodology assumes that each feeder vibrates with a statistically determined upper-bound velocity. The allowable velocity for each feeder is found by determining the lowest value of all the modal velocities based on allowable stress. If the minimum allowable velocity of all modes for a feeder is less than the upper-bound velocity, the feeder can not be defueled according to this method.

The purpose of this work is to develop a technique to improve quantification of the vibrational velocity of a specific feeder using the Fluid-Structure Interaction (FSI) capabilities of a commercial software package. The goal is to reduce the conservatism in the assumed vibrational velocity so that additional channels can be defueled. The first phase of this project recreated a published experiment with a FSI model and compared results. Later phases will apply the same FSI technique to actual feeder geometry, where the vibration velocity results are deemed overly conservative. This report documents the results of the first phase.

2. Validation case problem description

2.1 Test-apparatus overview

The validation case is obtained from [1]. This reference contains two separate cases, but only the first is used for validation. The system consists of a straight pipe suspended on long wires, sealed, and filled with water which is pressurized to prevent cavitation. The pipe is struck on one end by an impact rod which creates a compressive stress wave in the pipe and a high pressure wave in the liquid. A diagram of the test-apparatus is shown in Figure 1.

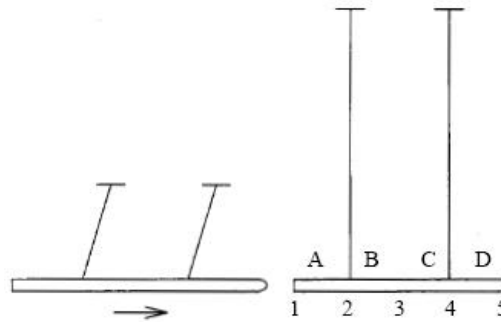


Figure 1 Test apparatus with impact rod (left) and water-filled pipe (right) with sensor locations shown [1]

2.2 Description of test-apparatus FSI

The impact of the rod on the pipe at point 1 causes an initial compressive stress wave in the pipe, S1, which travels at a speed of:

$$\text{Wave speed in solid} = c_s = \sqrt{\frac{E_s}{\rho_s}} = \sqrt{\frac{168[\text{GPa}]}{7985[\text{kg}/\text{m}^3]}} = 4587[\text{m}/\text{s}] \quad (1)$$

where E_s is Young's modulus of the pipe and ρ_s is the density.

This compressive stress wave travels the length of the pipe to point 5 in about 1 ms. A reflected tensile stress wave, S2, then travels back toward point 1. After a total time of roughly 2 ms, S2 reaches point 1 which causes separation of the impact rod from the pipe. The applied force is then removed for the rest of the experiment.

The compression of the pipe during impact causes an expansion of the pipe circumference due to Poisson ratio effects which locally increases the pipe volume and slightly decreases the water pressure. This phenomenon is called Poisson coupling. This slight decompression of fluid travels with the solid stress wave. This wave is analogous to the precursor waves which are sometimes observed in water hammer experiments [1].

The initial impact and axial compression of the pipe create a high pressure wave in the liquid, L1, to travel the length of the pipe at a speed of:

$$\text{Wave speed in liquid} = c_L = \sqrt{\frac{K_L}{\rho_L}} = \sqrt{\frac{2.14[\text{GPa}]}{999[\text{kg}/\text{m}^3]}} = 1464[\text{m}/\text{s}] \quad (2)$$

where K_L is bulk modulus of the water and ρ_L is the density.

It takes about 3 ms for L1 to reach point 5. Prior to this, a second liquid pressure wave L2 is produced by the reflected tensile stress wave S2 (at ~1 ms). S2 causes an axial elongation of the pipe which causes L2 to be very decompressive. In fact, L2 is the single-largest pressure wave in the entire experiment and is caused *entirely* by the combined interaction of the structure with the fluid. If FSI effects were not included (i.e., if two-way coupling was excluded), then L2 would be omitted and results would be altered.

A visualization of the waves and reflections in the pipe are shown in Figure 2. Further discussion of solid and fluid waves and their interactions can be found in [1-2].

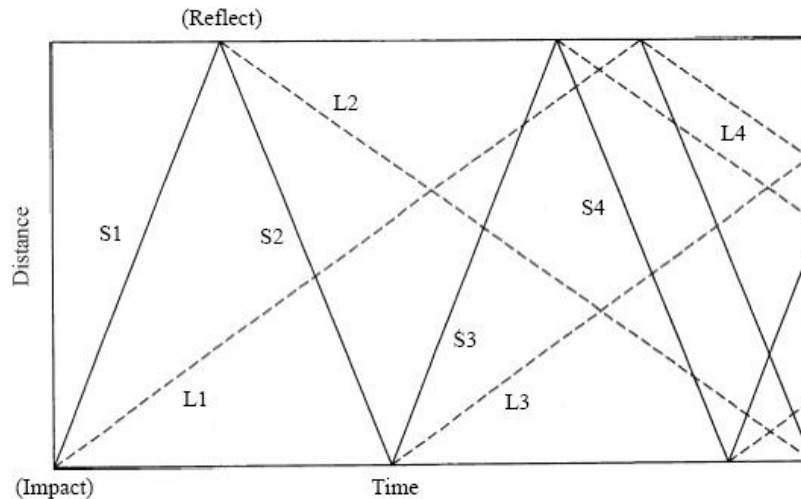


Figure 2 Stress waves (S) in pipe and liquid pressure waves (L) in water [1]

3. Modeling

3.1 Programs used

The two-way coupled FSI problems were solved with the ANSYS Multi-Field Solver (MFX). The physics of both the solid and fluid are set-up separately with the interface load transfer regions specified. In this model, the fluid regions transfer pressures to the solid which cause it to deform. These deformations are then transferred back to the fluid and alter the fluid response.

3.2 Geometry

The pipe geometry was modeled using the specifications given in [1]. It is 4502 mm long, 59.9 mm OD, 52.0 mm ID. The pipe model is perfectly straight; no bowing was taken into account.

The pipe is sealed and contains pressurized water to prevent cavitation. The exact specifications of the end caps were not given; however, their mass and length were provided. It is noted in [1] that both caps had negligible influence on any one event, but over long durations had a cumulative effect. Each cap was assumed to have the same density as the pipe.

Two planes of symmetry were applied to the geometry, which formed a 45° wedge shaped model.

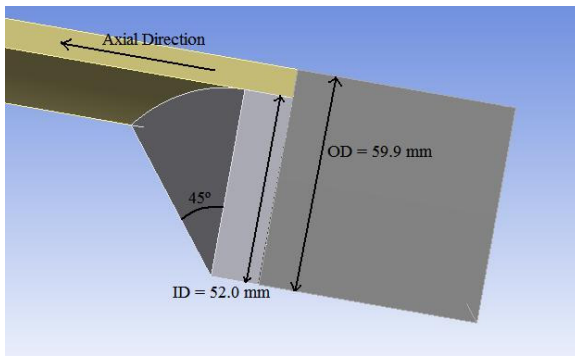


Figure 3 Impact cap geometry (45° model)

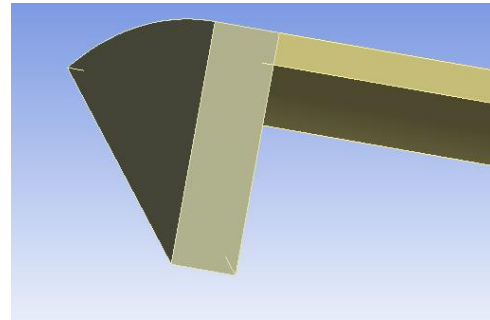


Figure 4 Remote cap geometry (45° model)

Figure 5 shows the fluid domain which fills the interior of the pipe. It was also modeled as a 45° wedge with a 52.0 mm outer diameter and length of 4491.2 mm. A portion of the fluid domain is shown in Figure 5.

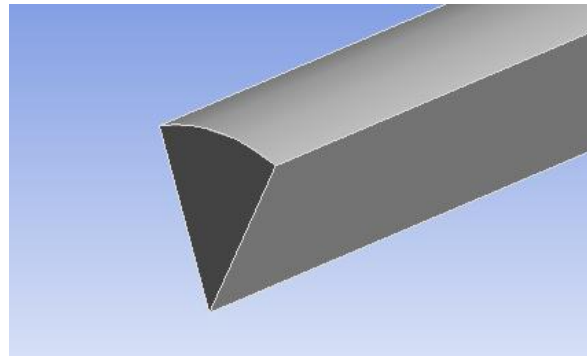


Figure 5 End portion of fluid domain (45° model)

3.3 Materials and model physics

The pipe and end cap materials were modeled as steel with Young's modulus, density, and Poisson's ratio of 168 GPa, 7985 kg/m³, and 0.29, respectively [1].

The water inside the pipe was modeled as a compressible fluid, with density a function of pressure:

$$\text{Density} = 998.32 \text{ [kg/m}^3\text{]} + \text{Pressure [Pa]} * 4.4265 \times 10^{-7} \text{ [s}^2\text{/m}^2\text{]} \quad (3)$$

This relation was based on steam table data obtained from [3]. The system was isothermal, and all properties were taken for 20 °C. Dynamic viscosity was 1.003 x 10⁻³ N-s/m² [4].

The solid region was modeled using large displacement, 20-node elements, and the fluid was modeled with a standard k-ε turbulence model with tetrahedral and prism elements. The system is 3-D, transient, and isothermal at 20 °C.

3.4 Boundary conditions

According to [1], flexural vibration bending in the pipe was negligible; therefore, two symmetry planes were used and only a 45° wedge of the pipe was modeled to take only axial vibration into account and reduce model size. The inside wall of the pipe and the base of both end caps were defined as solid-fluid interface. Fluid surfaces in contact with solids were also modeled as no-slip smooth walls.

3.5 Supports & loads

Lateral structural supports for the pipe (X and Y directions) were applied where the two symmetry planes meet in both of the end caps. These locations are coincident with the centre axis of the pipe which runs in the Z direction. The axial (Z) direction was unconstrained to permit translation of the pipe.

A stepped load was applied uniformly over the end cap face. In the experiment, the load was applied for the duration of time it took the initial pulse to return to the impact point and separate the pipe from the impact rod. The model simulation time was 1.96 ms for this condition which was subsequently rounded off to 2 ms for performing other convergence studies.

3.6 Timestep and mesh

The mesh size and timestep were based on a desired frequency of 5000 Hz. The major changes in pressure and strain have a period of about 1 ms, so a resolution of 0.2 ms was chosen. This choice of timestep adds a level of approximation which will not fully resolve the peak amplitude of some strong short waves.

To resolve the peaks with improved fidelity, it was recommended in [5] that a timestep of $1/180f$ be used, or $\sim 1.1 \times 10^{-6}$ s. Simulations were run with this small timestep, which showed some improvement in the response compared to larger timesteps, but not enough to justify the significantly longer run times. It is predicted that future phase modeling with smoother load application will not require such a fine timestep. The final timestep chosen for the results was 1×10^{-5} s.

The solid mesh size along the axial length was based on [5] where, in the case of wave propagation effects, the mesh should be fine enough to resolve the wave (about 20 elements per wavelength). For waves with a period of 0.2 ms traveling at 4587 m/s, the wavelength is 0.9174 m. Dividing the wavelength by 20 results in ~ 0.046 m per element. The final axial mesh length used is 0.04 m.

The circumferential direction was split into 3 sections, each with a 15° arc. The radial thickness of the pipe wall was divided into two elements. All solid elements were hexahedral. The solid mesh is shown in Figure 6.

The fluid mesh was made up of prism elements in the boundary layer mesh and tetrahedral elements for the rest of the volume.

Any radial gradients in the pipe were not expected to be very strong because the internal pipe flows are small and could probably be approximated by a 1-D model. No edge of any tetrahedral element exceeds 0.04 m in any direction, although the mesh could potentially be coarser since the wave speed of the fluid is about a third of the solid. The fluid mesh is shown in Figure 7.

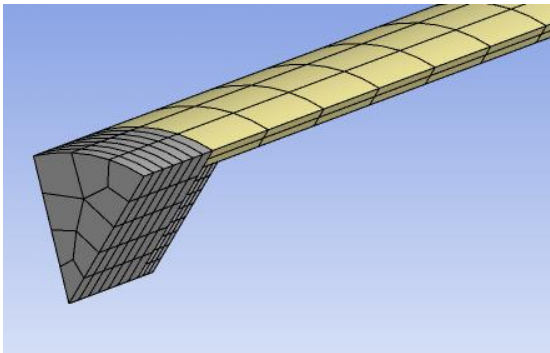


Figure 6 Solid mesh in impact cap region

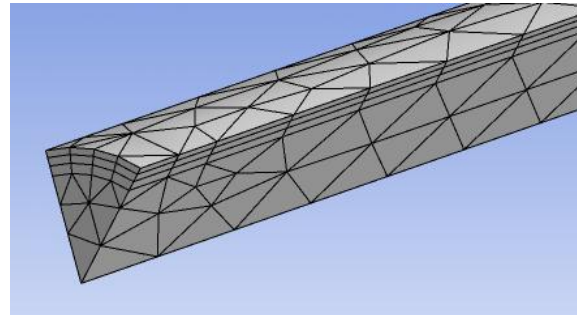


Figure 7 Fluid mesh in impact cap region

4. Results

The results obtained from the solution are presented below in Figure 8 to Figure 27. The sensor locations p1 to p5 provide the pressure results, v1 is the axial velocity of point 1, and sA to sD are the axial strain results. Experimental results are obtained from [1]. The sensor locations are shown in Figure 1.

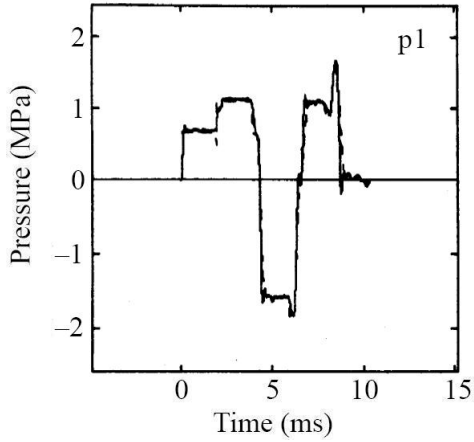


Figure 8 Experimental results of pressures at 1

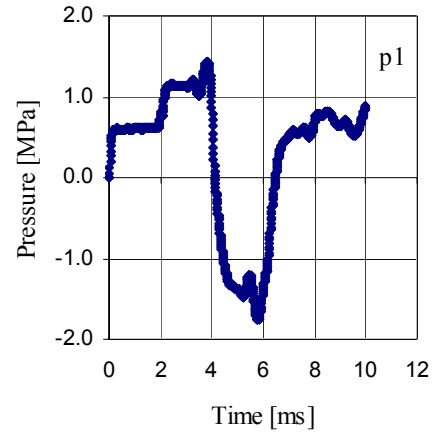


Figure 9 Computational results of pressures at 1

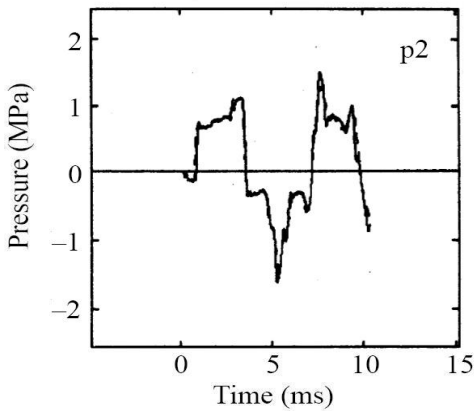


Figure 10 Experimental results of pressure at 2

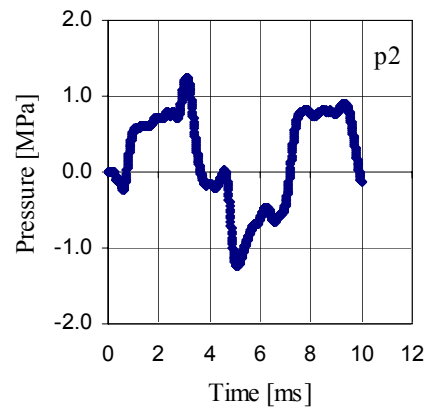


Figure 11 Computational results of pressure at 2

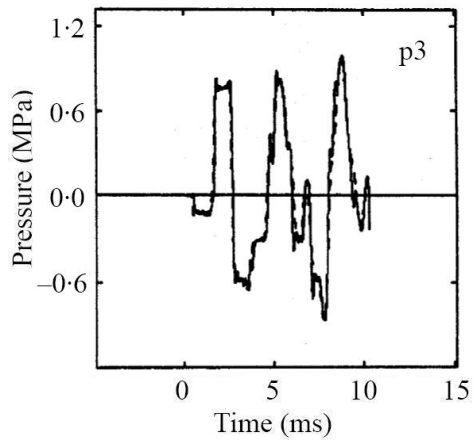


Figure 12 Experimental results of pressure at 3

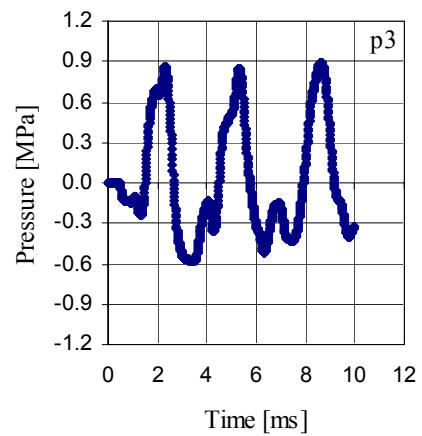


Figure 13 Computational results of pressure at 3

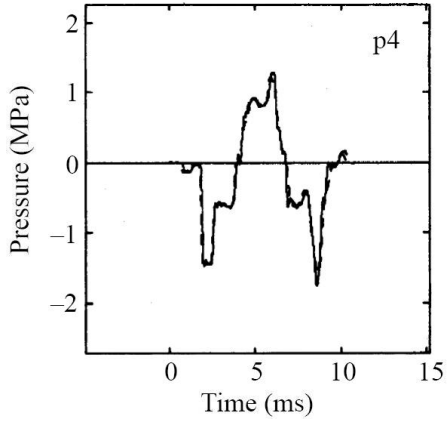


Figure 14 Experimental results of pressure at 4

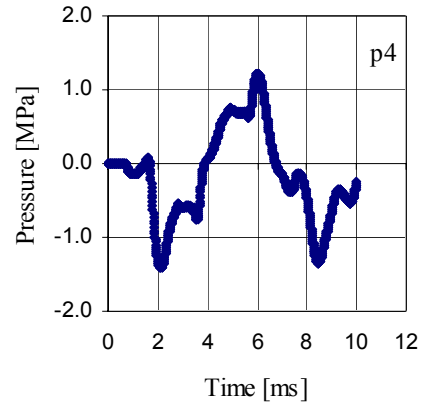


Figure 15 Computational results of pressure at 4

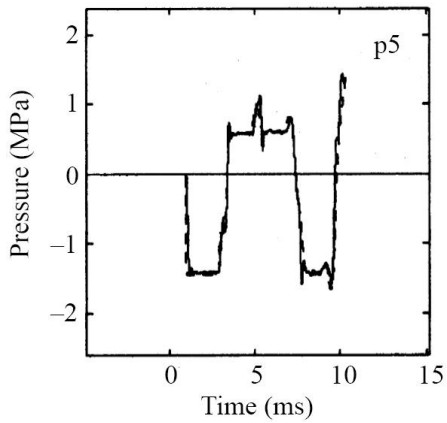


Figure 16 Experimental results of pressure at 5

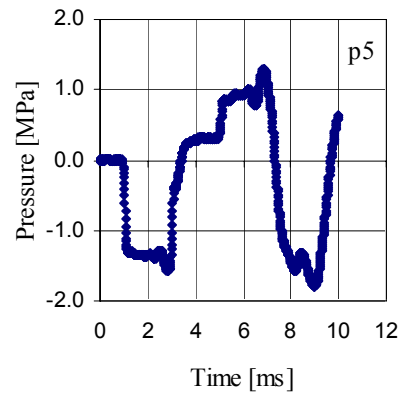


Figure 17 Computational results of pressure at 5

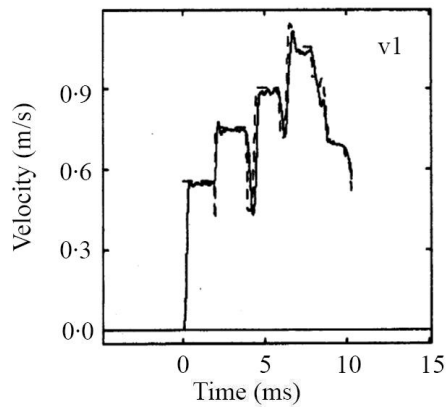


Figure 18 Experimental axial velocity of point 1

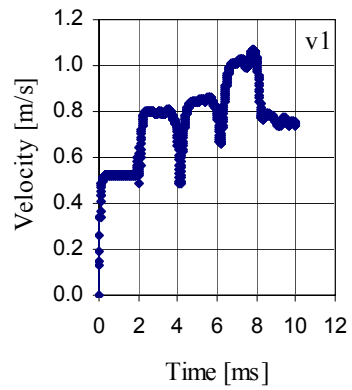


Figure 19 Computational axial velocity of point 1

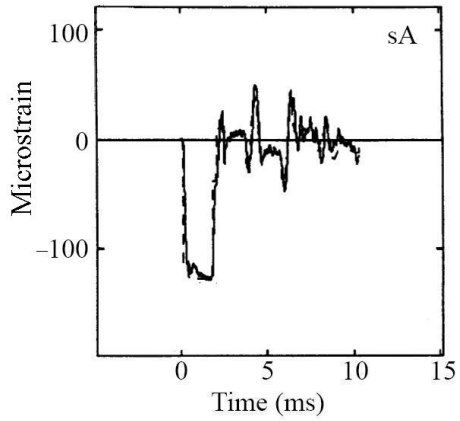


Figure 20 Experimental axial strain results at A

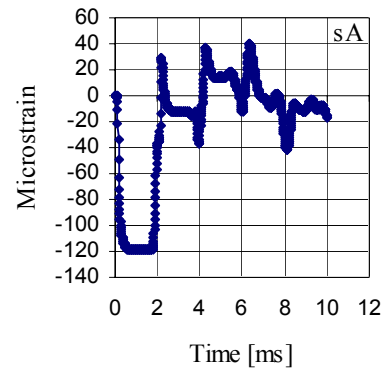


Figure 21 Computational axial strain results at A

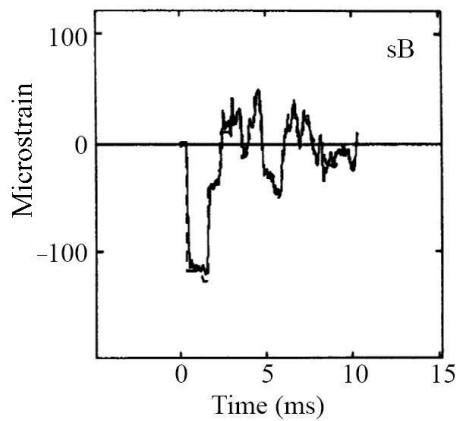


Figure 22 Experimental axial strain results at B

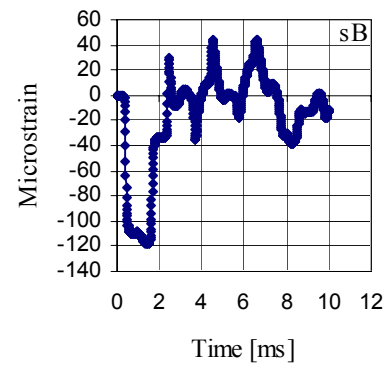


Figure 23 Computational axial strain results at B

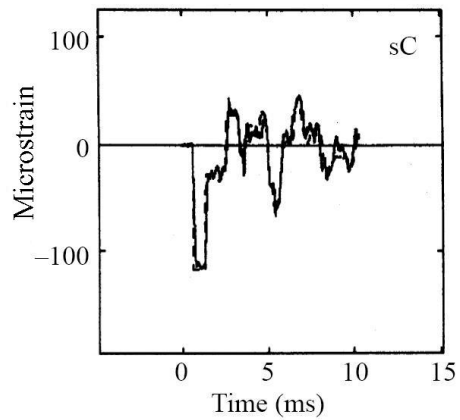


Figure 24 Experimental axial strain results at C

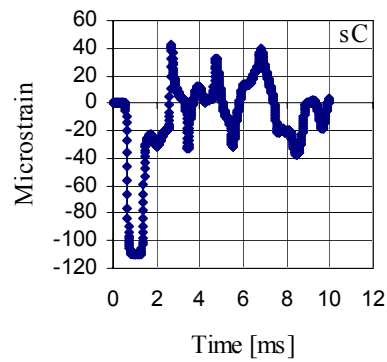


Figure 25 Computational axial strain results at C

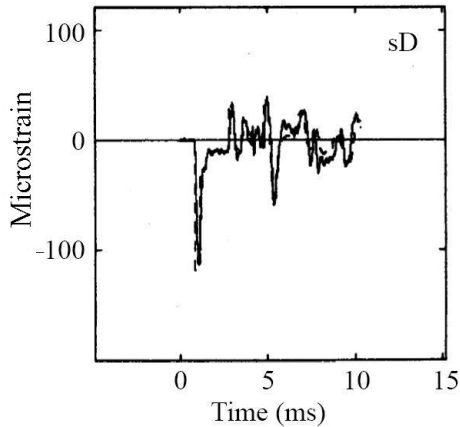


Figure 26 Experimental axial strain results at D

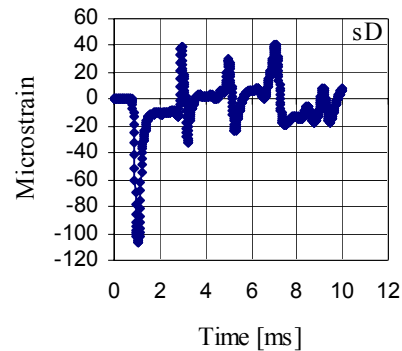


Figure 27 Computational axial strain results at D

5. Discussion

The methodology was successful in reproducing the FSI effects seen in the experimental case. The agreement between the results is very good, considering the relatively small effort spent on optimizing the various parameters due to time and budget constraints.

Most of the major FSI effects are present in the results. The strong pressure wave L2 can be observed, which would not have existed without two-way coupling of the two solutions. The precursor wave effect can be observed in Figure 11, Figure 13, and Figure 15. Other results support the accuracy of the model, such as the diminishing width of the initial negative strain pulse between S1 and S2 in Figure 21, Figure 23, Figure 25, and Figure 27. The pulse widths of the major waves appear to be closely replicated.

There are discrepancies in the results, and these could be due to a variety of reasons which include mesh coarseness, solution timestep, energy transfer, and geometry. It was observed in tests with larger timesteps that the peaks of the stepped input rounded off further. Large amplitude, short period pulses also did not reach the full amplitude with the larger timestep.

Perhaps the most significant inaccuracy is seen after the stress wave S5 is created at about 4 ms (see Figure 20 and Figure 21). The compressive S5 stress wave does not appear to have as large a magnitude as in the experimental results. This is most likely the reason for the p5 pressure discrepancy at 5 ms. The cause of this needs to be explored further to be fully understood. It may be due to the approximation of load duration, solid or fluid mesh discretization, or timestep. In the experiment, the pipe transfers momentum to the impact rod when it pushed it away. This energy loss from the pipe is not taken into account in the model, and could possibly play a role.

As time progressed further in both the experiment and predicted solution, the amplitude of the strains decreased and the results tend to become 'blurred' as a result of damping and fluid losses. This effect is not expected in the case of the feeder analysis because of

the cyclic loading; therefore the system should reach a state of periodic equilibrium. A suitable timestep and mesh density can then be chosen to resolve that state.

6. Conclusions

The results from the Phase 1 analysis show that the predicted results closely replicate the major features of the FSI phenomena found in an axial pipe wave propagation experiment. Future work with actual feeder geometry with known vibration velocity values will provide a better test case to determine the capabilities of this technique due to the smoother cyclic input load and more easily defined rigid and spring supports.

7. References

- [1] Vardy, A. E., Fan, D., and Tijsseling, A. S., "Fluid-Structure Interaction in a T-Piece Pipe", *Journal of Fluids and Structures*, Vol. 10, 1996, pp. 763-786
- [2] Tijsseling, A. S., "Fluid-Structure Interaction in Liquid-Filled Pipe Systems: A Review", *Journal of Fluids and Structures*, Vol. 10, 1996, pp. 109-146
- [3] Moran, M. J., and Shapiro, H. N., "Fundamentals of Engineering Thermodynamics", 4th Edition, John Wiley & Sons, Toronto, 2000
- [4] White, F. M., "Fluid Mechanics", 4th Edition, McGraw-Hill, Toronto, 1999
- [5] "ANSYS 11.0 Documentation" ANSYS Inc., 2007